Published in *Topics in Catalysis*, vol. 50, pp. 222-230 (2008)
The original publication is available at www.springerlink.com
http://www.springerlink.com/content/r547x728457h0653/

INFLUENCE OF AL DISTRIBUTION AND DEFECTS CONCENTRATION OF FERRIERITE CATALYSTS SYNTHESISED FROM Na-FREE GELS IN THE SKELETAL ISOMERISATION OF N-BUTENE.

Authors: *C. Márquez-Alvarez, A.B. Pinar, R. García, M. Grande-Casas and J. Pérez-Pariente**

Instituto de Catálisis y Petroleoquímica, CSIC, C/Marie Curie 2. Cantoblanco, 28049-Madrid, Spain

* e-mail: jperez@icp.csic.es

ABSTRACT

The skeletal isomerisation of n-butenes to isobutene has been carried out over ferrierite catalysts (Si/Al ~ 15) containing different acid sites distribution and different amount of defects. The zeolite crystals were synthesised under hydrothermal conditions in fluoride medium in the absence of alkaline cations by using suitable combinations of structure directing agents. Template-driven low density of acid sites in 10-membered-ring channels enhances the isobutene selectivity and decreases catalyst deactivation. The presence of high amount of silanol groups and Lewis acid sites increases the yields of by-products and catalysts decay.

Keywords: Ferrierite; zeolite synthesis; fluoride medium; Al sitting; acid sites distribution; FTIR; pyridine; isomerisation; 1-butene, isobutene

INTRODUCTION

The skeletal isomerisation of linear butenes to isobutene catalyzed by the zeolite ferierrite has been much investigated since its noticeable performance in this reaction was reported in 1990s [1-3]. A substantial number of contributions focuses on

mechanistic aspects of this reaction, for unimolecular and bimolecular mechanism have been proposed to take place inside the zeolite channels and to yield different products, in particular isobutene [4-9], on the deactivation mechanism of the reaction, as the selectivity to the targeted isobutene strongly enhances with time-on-stream and hence with catalyst deactivation [10-12], and on the contribution of the number, type and location of acid sites. Indeed, Brönsted acid sites can be located in different positions in the framework, either in the 10-MR channel or in the ferrierite cage accessible through 8-MR windows [13-16] and, moreover, the contribution of extra-framework Lewis acid sites has also been studied [17-19].

All these contributions reflect the complex nature of the reaction, and the combination of several factors that lead finally to selective catalysts. Among them, the location and type of acid sites seems to play a determinant role in the isobutene yield and in the deactivation process. A number of studies on the location of acid sites in H-ferrierite evidence that the protons are associated to framework oxygen atoms located at specific positions, which, together with the studies on adsorption of CO on Li-exchanged samples [20] point to a non-random distribution of Al in the framework. However, we have found recently evidences that the Al location in the framework can be influenced by the nature of the template used in the synthesis when this is carried out in the absence of sodium cations [21,22]. Different combinations of templates such as 1-benzyl-1-methyl-pyrrolidinium, pyrrolidine and tetramethylammonium led to samples exhibiting large differences in the fraction of Brönsted acid sites accessible to pyridine, which strongly affects the activity of these samples in acid-catalyzed reactions such as isomerisation/disproportionation of m-xylene and n-butene isomerisation.

An additional factor to take into account in determining the activity and selectivity of ferrierite catalysts arises from the potential presence of a high concentration of silanol groups as a function of specific synthesis conditions. In regard to this, it is worth mentioning that relatively well-defined crystalline layered aluminosilicate known as PREFER has been isolated and described, which led to three-dimensional ferrierite by condensation upon heating [23]. Mismatching of consecutive layers by shifting them along the plane perpendicular to the layer stacking prevents full condensation of all the available terminal SiOH groups present at the layer surface, which remain hence as connectivity defects in the final, partially condensed material. The so-called PREFER can be considered as an end-member of a family of layered materials related to ferrierite, to which many different materials with divers degree of layer condensation belong to, such as MCM-47, the borosilicate ERS-12 or the UZM series of materials [24-26].

We have reported elsewhere on the synthesis of ferrierite materials possessing different degree of layer condensation, and hence different concentration of connectivity defects (uncondensed SiOH groups), crystallised by using a proper combination of several cage-forming and channel-forming co-structure directing agents [27, 28]. Those synthesis procedures made available ferrierite crystals possessing various degrees of connectivity defects, which allow exploring in a systematic way the influence of this parameter on the skeletal isomerisation of n-butene. In this work, the study of the catalytic behaviour of these samples will be complemented with that of low-defect samples described above and reported elsewhere [21], which contain a non-random distribution of acid sites also obtained by appropriate choice of co-structure directing agents.

EXPERIMENTAL

Zeolite synthesis

Zeolites were synthesised from gels of molar composition: 0.06 Co-SDA: 0.48 ROH: 0.48 HF: 0.03 Al_2O_3: 0.94 SiO_2: 4.30-4.70 H_2O where ROH designates 1-benzyl-1-methyl-pyrrolidinium (bmp) hydroxide or (S)-2-hydroxymethyl-1-benzyl-1-methylpyrrolidinium (bmprol) hydroxide and co-SDA designates the corresponding co-structure directing agent used in each preparation: tetramethylammonium (TMA) hydroxide (Aldrich, 25 wt% aqueous solution), quinuclidine (quin) hydrochloride (Aldrich, 97 wt%), tetraethylammonium (TEA) hydroxide (Aldrich, 35 wt% aqueous solution). A sample prepared in the presence of pyrrolidine (pyrr) as the only SDA was crystallised from a gel with the same molar composition but with 0.54 moles of pyrrolidine (Aldrich, 99.5%). The reagents were used without subsequent purification.

In a typical preparation, 30.52 g of tetraethylorthosilicate (TEOS, Merck, 98 wt%) and 1.93 g of aluminium isopropoxide (Fluka, 97 wt%) were added to a solution containing 35.1 g of bmprol hydroxide and 3.3 g of tetramethylammonium hydroxide. The solution was left under stirring until the ethanol and the excess of water were evaporated. Subsequently, 3.06 g of HF (Panreac, 48 wt%) were added dropwise. The resulting thick gel (pH ~9.7) was homogenized and introduced into 20-mL Teflon-lined stainless steel autoclaves, which were heated statically at 135 ºC under autogeneous pressure for selected periods of time. The solid products were recovered by filtration, washed with water and ethanol and dried at room temperature overnight.

The organic compounds occluded in the as-made crystals were removed by calcination. For this purpose, the zeolite samples were heated in N_2 up to 200 °C and maintained at this temperature for 2 h, followed by treatment with a flow of ozone/oxygen (60

mL/min, ca. 2 vol% O_3) at 200 °C until complete removal of the organic material. Ozone in oxygen stream was produced using an ECO-5 ozone generator manufactured by SALVECO Proyectos S. L. Prior to their use in catalysis, the sample were heated in air for two hours till the temperature reached 550 ºC and kept at that temperature for two hours.

A sample synthesised with pyrrolidine as SDA at high pH and in the presence of sodium cations was prepared following the procedure of Plank et al. [29]. It was ion-exchanged and calcined as described in reference [21].

The samples will be referred to with the name of the organic molecules employed as SDAs in each case, separated by a dash and followed by the duration of the hydrothermal treatment when it is necessary to specify it. As an example, FER-bmp-quin-10d was obtained after crystallisation for 10 days using 1-benzyl-1-methyl-pyrrolidinium and quinuclidine as SDAs.

Characterisation

Solid products were characterised by XRD (PANalytical X´Pert PRO-MPD diffractometer. CuKα radiation), thermogravimetric analysis (Perkin-Elmer TGA7 instrument, heating rate 20 ºC/min, air flow 30 mL/min, temperature range 20-900 ºC), chemical CHN analysis (Perkin-Elmer 2400 CHN analyzer) and SEM/EDX (Jeol JSM 6400 Philips XL30 operating at 20 kV). Nitrogen adsorption-desorption isotherms were measured at -193 °C using a Micromeritics Tristar 3000 volumetric apparatus. Specific surface areas were calculated following the BET procedure.

FTIR spectra in the transmission mode were recorded in the 1000-4000 cm^{-1} range, at 4 cm^{-1} resolution, using a Nicolet 5ZDX and a ThermoNicolet Nexus 670 FTIR spectrometers provided with MCT detectors. The samples were pressed into self-

supporting wafers (ca. 6 mg/cm^2 thickness), placed in a glass cell with CaF_2 windows, and activated in vacuum at 400 ºC for 8 h. Pyridine adsorption was carried out on activated samples kept at 150 ºC, and followed in dependence of time. The sample wafer was put in contact with pyridine vapour (8 Torr) at 150 ºC for a given period of time, subsequently degassed at the same temperature for 30 min, and then the FTIR spectrum was recorded. Pyridine was again dosed into the cell to allow further adsorption of the amine on the sample wafer, and the cell was evacuated for 30 min prior to recording the FTIR spectrum. This adsorption procedure was repeated several times in order to obtain a series of FTIR spectra at increasing total contact time of the sample wafer with pyridine. The spectra recorded after pre-treatment and after every pyridine adsorption step were normalised to a sample thickness of 6 mg/cm^2. Difference spectra in the pyridine ring vibrations region were obtained by subtracting the spectrum of the pre-treated sample.

Catalytic activity test

The transformation of 1-butene was carried out in an automatic fixed-bed reactor under the following conditions: 400 ºC, atmospheric pressure, N_2/butene molar ratio = 4, weight hourly space velocity (WHSV) = 25 h^{-1}. The catalysts samples ≈ 100 mg (pelletised and sieved to 0.42-0.84 mm) were previously pre-treated in situ under nitrogen flow for 1 hour at 400 ºC. The products were analysed on-line by gas chromatography using a capillary column (PLOT Al_2O_3 50 m x 530 μm). A Varian Cp-3880 gas chromatograph provided with a flame ionisation detector (F.I.D.) was used in the analysis. The conversion into the different products was calculated by considering n-butene isomers as the reactant.

RESULTS AND DISCUSSION

Synthesis and bulk characterisation

For the sake of clarity, the as-synthesised ferrierite samples have been classified into two different groups, according to their XRD pattern. These have been denoted as "Ferrierite-type materials" and "fully condensed ferrierite crystals", for samples having broad and poorly defined XRD peaks, in the first case, and those presenting a set of narrow peaks characteristic of conventional ferrierite crystals, for the latter.

Fully condensed ferrierite crystals

To study the effect of the combination of the different SDAs employed in the synthesis on the acid site distribution of the resulting materials, we carried out experiments using TMA+bmp, TMA+pyrrolidine and pyrrolidine alone in fluoride medium, and pyrrolidine in alkaline medium. Zeolite ferrierite was obtained in all these syntheses, as shown by the XRD patterns, although the FER-bmp-TMA sample presented somewhat broader diffraction peaks than the others. Scanning electron microscopy showed that these FER-bmp-TMA solids are composed by neddle-like crystals of about 7 microns in length, similar to those present in the ferrierite-type materials, as it will be shown below. By contrast, the samples obtained in the absence of bmp are composed of agglomerates of plate-like crystals. Differences in crystal size are observed among these samples. FER-pyrr and FER-pyrr-TMA samples possess crystals of about 22×13 microns, whereas those of FER1 sample prepared in alkaline medium have dimensions of about 2×2.5 microns.

The Si/Al ratio as measured by SEM/EDX corresponds to an aluminium content of ca. 2.2 atoms per unit cell of ferrierite, without substantial differences between the several samples.

For the samples prepared with pyrrolidine or pyrrolidine and TMA, the resulting C/N ratio was 4, close to the theoretical value corresponding to these molecules [21]. Chemical analysis and ^{13}C CP MAS NMR confirmed the integrity of TMA and bmp cations after the hydrothermal treatment for the FER-bmp-TMA samples [30].

Chemical analysis showed an organic content between 8.5 and 13 wt%, depending on the molecules employed as SDAs in each case.

Ferrierite-type of materials

To study the role of the structure directing agents in the synthesis of ferrierite materials, we have systematically increased both the size of the large SDA and that of the smaller co-SDA. In a first set of experiments, the co-SDAs were varied using molecules of different sizes and shapes in preparations with bmp as the bulky SDA. Hence, the initial TMA cation was systematically substituted by a similar though bigger cation, TEA, and the cyclic bulkier amine quinuclidine. In a second step, to test the effect of a change in the large cation, bmp was replaced by a related although slightly bulkier cation, bmprol, in the preparation with TMA as a co-SDA.

Table 1 summarises the gel compositions and the products obtained in these preparations. The corresponding XRD patterns are depicted in Figure 1. The X-ray diffraction pattern of a sample of ferrierite synthesised with pyrrolidine (FER-pyrr-10d) corresponding to a fully condensed ferrierite material is also shown for comparative purposes.

The diffraction patterns of all the samples are very similar and indicate that the products are related to the family of ferrierite layered materials. As commented in the introduction, these solids possess a structure made up by the stacking of ferrierite sheets along the direction perpendicular to the layer with the organic molecules used as SDAs located in the interlayer space. The different arrangement of the ferrierite sheets gives rise to the different members of this family of materials like PREFER [23] or MCM-47 [24].

The main difference among the XRD patterns of the as-synthesised products obtained in this study lays on the position of the first diffraction peak, which corresponds to the (200) planes of the structure and therefore is related to the interlayer distance. This distance varies with the specific combination of SDA and co-SDA employed in synthesis, as can be seen in Figure 1(1). This is in line with our hypothesis that the formation of the layered phases in this system is caused by the different fitting of the co-SDAs within the ferrierite cages, hindering the complete condensation of adjacent ferrierite sheets, as has been reported in ref. [27]. A particular case concerns the materials prepared with quinuclidine, that shows a shift of the (200) reflexion with the crystallisation time, which has been attributed to the exchange of the organic SDAs as the crystallisation proceeds, resulting in materials richer in bmp at short crystallisation times and in materials richer in quinuclidine for longer times of synthesis [27]. Indeed, ^{29} Si MAS NMR shows the presence of a high amount of silanol groups (Q3) in this sample, evidencing the incomplete condensation of ferrierite layers [27]. Another evidence that suggests the presence of a high amount of uncondensed silanol groups in these samples is their high content of occluded organic material, which is between 15 wt% and 18 wt% (Table 2), depending on the sample. This amount is much higher than that of fully condensed ferrierite crystals discussed above (Fig.2 and Table 2), and this

excess of organic material should be located at interlayer regions associated to Q3 silicon atoms. Indeed, it can be seen also in Table 2 that the TG weight loss at T > 200 ºC is higher than the total organic content as determined by chemical analysis. This excess would correspond to the release of water coming from the condensation of silanol groups present in the solid. From this point of view, it is interesting to notice that the FER-bmprol-TMA samples possesses an organic content of ca. 13 wt%, according to chemical analysis, which is lower than that of the other materials. Hence, this sample might constitute an intermediate case between the fully condensed ferrierite crystals and the highly uncondensed ferrierite-type materials.

After calcination, the samples show similar X-ray diffraction patterns as a result of the removal of the organic content between the layers and the partial condensation of the silanol groups of consecutive layers (Figure 1(2)). This is manifested by the shift of the (200) diffraction to higher 2θ values, particularly for the materials prepared with bmp and quinuclidine or TEA as co-SDAs. The solid synthesised with bmprol and TMA, does not seem to possess a layered structure similar to that of the samples crystallised with bmp and quinuclidine or TEA, since calcination of the material does not shift the lower-angle diffraction peak as much as in the former cases.

Scanning electron microscopy revealed a similar crystal size and morphology for the samples synthesised with bmp and different co-SDAs. These solids crystallised as aggregates of long needles of around 5-10 x 0.3-0.5 μm in size. The sample synthesised with bmprol shows a slightly different crystal shape and also possesses lower amount of amorphous material. The Si/Al ratio of the samples (Table 1) is close to that of the nominal value of the gel (Si/Al=15), although this ratio is slightly higher for the samples synthesised with TEA (Si/Al=18.6).

The textural properties of the calcined samples are summarised in Table 2. The higher BET areas correspond in general to the layered ferrierite materials, which could indicate that after calcination the layers are not completely condensed, in agreement with the IR results that will be discussed in the next section.

FTIR characterisation of surface groups

The O-H stretching region of the FTIR spectrum of sample FER-bmp-TMA outgassed at 400ºC is shown in Figure 3 (a). The spectrum is similar to those of the other fully condensed ferrierite samples obtained in fluoride medium that have been reported elsewhere [21], and exhibits an intense asymmetric band at ca. 3601 cm^{-1} with a weak shoulder at 3550 cm^{-1}, characteristic of bridging hydroxyl groups (Si-OH-Al), and a weaker band at 3747 cm^{-1}, corresponding to terminal silanols. Upon contact with pyridine at 150 ºC for 90 min (and subsequent removal of physically adsorbed pyridine in vacuum at 150 ºC for 30 min), it is observed a decrease of the intensity of both the terminal silanol and the bridging hydroxyl bands. Concomitantly, several bands corresponding to pyridine ring vibration modes appear in the 1700-1400 cm^{-1} range (Figure 3, right). The strong bands at 1545 and 1638 cm^{-1} are assigned to pyridinium cations, the weak band at 1455 cm^{-1}, to pyridine interacting with Lewis sites, and the weak bands observed at 1445 and 1596 cm^{-1} are assigned to pyridine hydrogen-bonded to silanol groups [31, 32]. Furthermore, bands at 1620 cm^{-1} and 1490 cm^{-1} are observed, to which pyridine species interacting with both Brönsted and Lewis sites contribute. It can be observed in Figure 3 that the formation of pyridinium ions produces only a partial removal of the bridging hydroxyl band (3601 cm^{-1}). It has been previously reported [21] that prolonging pyridine contact at 150 ºC slightly decreased the intensity of the bridging hydroxyl band, although the band still retained a large fraction of its

original intensity after contact with pyridine for 4 h. It was concluded that only a part of the strong Brönsted acid sites are accessible to pyridine at 150 ºC in all the fully condensed ferrierite samples, and that accessibility was dependent on the combination of organic molecules used as SDAs. Table 3 collects the estimated fraction of strong Brönsted sites accessible to pyridine for these samples and the relative concentration of Brönsted and Lewis sites probed by pyridine (expressed as normalised area of the corresponding IR bands). The samples show noticeable differences in Brönsted sites accessibility, although some disagreement is observed between this parameter and the concentration of pyridinium ions, which suggests differences in the total concentration of Brönsted sites among the samples. The weak intensity of the band at 1455 cm^{-1} shows that these samples possess a low content of extra-framework aluminium, being samples FER-bmp-TMA and FER1 those exhibiting the highest intensity for this band.

The FTIR spectra of the poorly condensed samples synthesised in fluoride medium, outgassed at 400 ºC show marked differences with respect to the spectra of the fully condensed ones. For the samples obtained substituting TMA by TEA or quinuclidine as co-SDA in the syntheses with bmp (Figure 3, c-e), the terminal silanol band exhibits higher intensity, in agreement with the expected higher concentration of silanols in these samples. This band shows a marked broadening which can be attributed to extensive hydrogen-bonding between neighbouring silanol groups, probably due to close proximity between silanol groups in two adjacent non-fully condensed ferrierite layers. Furthermore, the spectra show broad shoulders at ca. 3700 and 3650 cm^{-1}, that might be derived from Lewis extra-framework species [8, 11]. All these features suggest the presence of a large number of condensation defects in these samples. Furthermore, these samples exhibit much lower intensity (up to one order of magnitude lower) for the band corresponding to bridging Si-OH-Al groups. However, pyridine adsorption shows

that the concentration of Brönsted acid sites able to protonate pyridine is similar for all the samples synthesised with bmp and different co-SDAs (Table 3). After pyridine adsorption at 150 ºC for 5 min, the band at 3600 cm^{-1} was partly removed, its intensity was hardly decreased after contact with pyridine for 30 min, and remained constant at longer contact time (Figure 3, c-e, left). Despite the much lower intensity of the bridging hydroxyl band, and that only part of these sites are accessible to pyridine, the integrated area of the band due to pyridinium species is comparable to that of FER-bmp-TMA. This result suggests that only those Si-OH-Al species located in fully connected crystalline environments of ferrierite would give rise to the band around 3600 cm^{-1}. On the other hand, non-fully connected zeolite units would allow for a large variety of T-O-T angles and, hence, the Si-OH-Al species associated to these sites would not exhibit a well-defined vibration frequency of the hydroxyl group. A further evidence that supports this conclusion is given by the changes observed in the FTIR spectra of samples FER-bmp-quin at different crystallisation times. Increasing the duration of the hydrothermal treatment from 10 to 30 days is known to lead to a higher degree of condensation of the ferrierite layers [27], and this change is accompanied by a decrease of the intensity of the silanol band and an increase of the bridging hydroxyl band. It is worth to note also that the pyridinium band (1545 cm^{-1}) is significantly broader for samples FER-bmp-TEA and FER-bmp-quin as compared to FER-bmp-TMA, which also suggests a higher heterogeneity of the Brönsted acid sites of the former samples. According to the previous interpretation of the FTIR results, accessibility of pyridine to the Brönsted sites could not be directly related to the decrease of intensity of the band at 3600 cm^{-1} in the case of partly condensed ferrierite-type samples. Pyridine adsorption also shows a markedly higher concentration of Lewis sites for samples FER-bmp-TEA and FER-bmp-quin (Table 3). Finally, it can be

observed in Figure 3 that, for these samples, there is a progressive increase of the intensity of bands assigned to hydrogen-bonded pyridine, with a concomitant decrease of the silanol bands, with increasing time of pyridine adsorption. This result suggests that access of pyridine to the silanol groups is constrained, revealing a high tortuosity of the interlayer spacings created by partial condensation of the ferrierite sheets. It can also be observed that prolonged contact with pyridine also leads to an increase of the shoulder at 3650 cm^{-1} attributed to Al-OH species [33-35], mainly for samples FER-bmp-TEA and FER-bmprol-TMA, which origin is not clear at present.

The results of the FTIR characterisation discussed above support the conclusion that substitution of TMA by bulkier co-SDAs (TEA and quinuclidine) in the syntheses using bmp as SDA, lead to materials that retain a large number of condensation defects after calcination. In contrast, replacement of bmp by bmprol while keeping TMA as co-SDA seems to produce much less noticeable changes in the condensation degree of the calcined samples, in agreement with results shown above. The spectrum of pretreated sample FER-bmprol-TMA is similar to that of FER-bmp-TMA, showing a slightly more intense silanol band of similar width, and a slightly less intense Si-OH-Al band (Figure 3). The concentration of Lewis sites determined by pyridine adsorption is also close between these two samples. On the other hand, the amount of Brönsted acid sites accessible to pyridine in sample FER-bmprol-TMA seems to be nearly twice the amount in FER-bmp-TMA, based on the intensity of the pyridinium band (Table 3).

It can be concluded that, after calcination, samples synthesised using pyrrolidine in alkaline medium and, either alone or with TMA as co-SDA, in fluoride medium can be considered as ferrierite samples with low number of defects. Zeolites synthesised with TMA and either bmp or bmprol would belong also to this group, although the samples seem to possess an increased number of defects in the following order: FER-pyrr-TMA

< FER-bmp-TMA < FER-bmprol-TMA. On the other hand, replacement of TMA by the bulkier co-SDAs TEA and quinuclidine in the syntheses carried out with bmp leads to samples with a high content of condensation defects.

Catalytic activity

Low-defect samples

Tables 4 and 5 collect reaction conversion expressed as that of all n-butene isomers, 1-, 2- trans and 2-cis, for double bond shift and cis-trans isomerisation of n-butenes reach the equilibrium and they are much faster than skeletal isomerisation. Selectivity to the different reaction products of several catalysts for two different time-on-stream (t.o.s.), 5 and 720 minutes is also reported. The dependence of n-butene conversion, selectivity and isobutene yield on t.o.s. are depicted in Figures 4 and 5 for low- and high-defect samples, respectively. Nonetheless, data corresponding to the low-defect sample FER-bmprol-TMA have been plotted in Fig. 5 for comparison purposes.

Several features can be observed in Tables 4 and 5. First, at t.o.s. of 5 minutes, the conventional catalyst (FER1) presents the highest conversion, but the lowest isobutene selectivity. For all the catalysts, the yields of the two other major products, $C3^{=}$ and $C5^{=}$, are quite close to each other, which evidences that they are formed via butene dimerisation-cracking.

A yield to C6 higher than that to C7 is obtained for the conventional catalyst, opposite to what is obtained for the catalysts synthesised in fluoride medium. Finally, minor amount of n- and i-butane are formed, followed in decreasing order by ethylene, propane and C5.

For all catalysts, the conversion decreases as a function of t.o.s. (Figure 4) but marked differences in the deactivation pattern are observed among them, depending upon the

synthesis method of the ferrierite crystals. For the conventional catalyst, an activity loss of 70% is obtained after 720 minutes of t.o.s., while the selectivity to isobutene increases from 24% to only 38%, and the dimerisation/oligomerisation of butene followed by cracking still contribute notoriously to the overall butene conversion. In contrast to this behaviour, the samples obtained with TMA-bmp or TMA-bmprol (Table 4) not only posses a higher initial selectivity to isobutene (t.o.s. = 5 minutes), but also deactivate at lower rate (Figs. 4 and 5). Indeed, while the yield to isobutene only decreases slightly after 13h of run, the butene oligomerisation is suppressed in more than 90% in that period of time, which results in a selectivity to isobutene higher than 90%. Then, the selective deactivation of the oligomerisation/cracking pathway with t.o.s. is the main contributor to the activity decay. It is particularly noticeable the behaviour of the sample synthesised from TMA and bmp at long crystallisation time (83 days), which exhibits the highest isobutene yield, and presents the lowest deactivation rate (Figure 4).

Samples synthesised in fluoride medium from gels containing pyrrolidine are much less active, and, although the highly deactivated samples present a good selectivity to isobutene, this decreases very rapidly with the conversion (Figure 4), and therefore a very low isobutene yield is obtained at high t.o.s.

These results evidence that the main pathway for isobutene formation on these catalysts is the monomolecular skeletal isomerisation of n-butene. In order to explain these results, it has to be considered first that only a fraction of acid sites are interacting with adsorbed pyridine, as it is shown in Table 3, and those sites should be located in the 10-MR channel and would be engaged in n-butene activation [18, 36]. As it has been discussed elsewhere [21], the location of Al sites in the framework is a function of the particular combination of co-structure directing agents incorporated into the crystals.

The presence of TMA and pyrrolidine in the ferrierite cage is directing the Al sitting toward this cage, which give rise to the formation of acid sites non available to interact with the n-butene molecule. This effect of "pumping" aluminium into cage sites has as a consequence that less aluminium would be available to occupy accessible 10-MR channel sites, which strongly reduces the acid site density in those channels. Therefore, the actual Si/Al ratio in the channels must be much lower than the average Si/Al ratio of the whole crystals. This decrease in acid sites density at the channels should greatly decrease the catalyst ability to promote non-selective bimolecular dimerisation/oligomerisation reactions.

The beneficial effect of lowering the number of acid sites of ferrierite on isobutene selectivity has been reported by several research teams [17, 37], which has also been extended to MCM-22 catalysts [38]. However, these procedures require either the synthesis of ferrierite crystals with a very high Si/Al ratio, which has a detrimental impact on catalyst activity, or dealumination procedures that require additional steps to remove extra-framework aluminium species [17] that otherwise would produce a deleterious effect on both activity and selectivity.

In spite of acid sites location and density, some other effects might contribute to the observed overall catalytic pattern. For the two samples synthesised from pyrrolidine-containing gels in fluoride medium, their large crystal size could eventually contribute to faster catalyst deactivation, due to severe pore blocking of the channels by coke deposits. However, it has also to be considered that ferrierite catalysts with ca. 20 microns crystal size (Si/Al = 14.4) prepared from 1,4-diaminobutane in the absence of inorganic cations have been reported to show n-butene conversion higher than that of ferrierite with small crystal size and they are also more selective to $C3^{=}$ and $C5^{=}$ [12]. Moreover, these authors argued that the remarkable isobutene selectivity of aged H-

ferrierite could be correlated with the density of the Brönsted acid sites located near the 10-ring pore mouth, which is in agreement with the effect reported here on the influence of SDA on Al location.

It is also to notice the remarkable increase of isobutene yield obtained by increasing the crystallisation time in the TMA/bmp gel from 20 to 83 days. It can be observed in Table 2 that the amount of organic material occluded inside the crystals decreases with crystallisation time, and hence the catalyst would have less concentration of silanol defect groups. From this observation, it could be eventually concluded that the presence of such defects might be detrimental for catalysts selectivity to isobutene. This aspect has been further explored in more detail in the samples that contain a very high amount of silanol groups, as described below.

High-defect samples

Another factor influencing catalyst performance to which attention has been paid concerns the presence of Lewis sites and connectivity defects, i.e., silanol groups. The ferrierite samples described so far contain very little extra-framework aluminium, and a low amount of SiOH groups, which is not surprising owing to the fact the synthesis has been performed in fluoride medium [39]. However, the materials synthesised from a combination of bmp with either quinuclidine or TEA shows a much higher concentration of silanol groups as well as Lewis sites, as it has been discussed in previous section, and this produces noticeable changes in the pattern of catalytic n-butene transformation. Table 5 collects the activity and products selectivity of several high-defect samples for t.o.s. of 5 and 720 minutes, while the dependence of n-butene conversion, selectivity and isobutene yield on t.o.s. is depicted in Figure 5. The most noticeable difference with respect to the samples having low-defect concentration is the

fast decay of catalyst activity of the high-defect ferrierite catalysts. After 12h of run, the residual activity is between 15% and 25% that of t.o.s. = 5 minutes, depending on the type of catalyst. It is also noteworthy that, for the samples synthesised from quinuclidine-containing gels, the sample obtained at longer crystallisation time is more resistant toward deactivation, and, as it was discussed above, it indeed contains less amount of defects. For all these high-defect samples, the selectivity to isobutene is always below 80%, and poor yields to this product are obtained at high t.o.s., which are lower than 5% already after 12 h of reaction.

Although the presence of a high amount of silanol groups correlates with both high activity decay rate and low isobutene selectivity, it has to be taken into account that, as it was discussed in the previous section, an intense pyridine band associated to Lewis sites is also observed for these catalysts, its intensity increasing with that of the band attributed to silanol groups. It has been reported elsewhere that the simultaneous presence of Lewis and Brönsted sites in ferrierite catalysts enhances di-, oligomerisation/cracking reactions, leading to higher yields of by-products [18]. We are observing the same trend towards increasing by-products formation as far as the presence of Lewis sites proven by pyridine adsorption is concerned, but the detection of the two Lewis bands, and the simultaneous detection of high amount of defects silanol groups, preclude, in our opinion, a clear conclusion on the individual contribution of both chemical species to catalysts performance, i.e., extra-framework species coming from framework dealumination and silanol groups.

It is also interesting to observe that there seems to be a threshold value of defect content (contributed by extra-framework aluminum and silanol chemical species) in regard to the influence of this parameter on catalysts performance. Indeed, the sample FER-bmprol-TMA contains an intermediate amount of silanol groups and Lewis sites, which

is higher than that present in the samples synthesised from either bmp of pyrrolidine-containing gels. However, the isobutene yield (Table 5) is even higher than that obtained from the latter, whereas it is also more resistant toward deactivation (Figure 5).

CONCLUSIONS

The activity in the transformation of n-butenes and selectivity to isobutene of ferrierite catalysts can be greatly improved by synthesising the zeolite crystals in the presence of appropriate combination of structure directing agents in the absence of alkaline cations. These specific combinations of SDA allow to exert an effective control on the density of acid sites located at the 10-MR channel, where the reaction takes place. For SDA too bulky to be occluded in the ferrierite cage, a high amount of both silanol defects and Lewis acid sites are found in the resulting catalysts. The presence of such type of sites enhances the formation of by-products and promotes in a great extension catalysts deactivation.

Acknowledgements

We are thankful for the financial support of the Spanish Ministry of Science and Innovation (MICINN, former MEC), project CTQ2006-06282. A.B.P. acknowledges the Spanish MICINN for a predoctoral grant. R.G. acknowledges the J.A.E. contract (CSIC).

REFERENCES

1: P. Grandvallet, K. P. de Jong, H. H. Mooiweer, A. G. T. G. Kortbeek, B. Kraushaar-Czarnetzki, European Patent EP501577 (1992).

2: H. H. Mooiweer, K. P. de Jong, B. Kraushaar-Czarnetzki, W. H. J. Stork, S. C. Krutzen, Stud. Surf. Sci. Catal. 84 (1994) 2327.

3: J. Houzvicka, V. Ponec, Catal. Rev. Sci. Eng. 39(4) (1997) 319.

4: W.-Q. Xu, Y. –G. Yin, S. L. Suib, C.-L. O' Young, J. Phys. Chem. 99 (1995) 758.

5: P. Meriaudeau, R. Bacaud, L. N. Hung, T. A. Vu, J. Mol. Catal. A 110 (1996) L 177.

6: K. P. de Jong, H. H. Mooiweer, J. G. Buglass, P. K. Maarsen, Stud. Surf. Sci. Catal. 111 (1997) 127.

7: J. Čejka, B. Wichterlová, P. Sarv, Appl. Catal. A 179 (1999) 217.

8: B. de Ménorval, P. Ayrault, N. S. Gnep, M. Guisnet, J. Catal. 230 (2005) 38.

9 : M. Kangas, J. Villegas, N. Kumar, T. Salmi, D. Yu. Murzin, F. Sandelin, E. Harlin, Catal. Today, 100 (2005) 363.

10: M. Guisnet, P. Andy, N.S. Gnep, C. Travers, E. Benazzi, Stud. Surf. Sci. Catal. 105 (1997) 1365.

11: S. van Donk, E. Bus, A. Broersma, J.H. Bitter, K.P. de Jong, Appl. Catal. A 237, (2002) 149.

12: S.-H. Lee, C.-H. Shin, S.B. Hong, J. Catal., 223 (2004) 200.

13: J.A.Z. Pieterse, S. Veefkind-Reyes, K. Seshan, L. Domokos, J.A. Lercher, J. Catal. 187 (1999) 518.

14: A. Martucci, A. Alberti, G. Cruciani, P. Radaelli, P. Ciambelli, M. Rapacciulo, Microporous Mesoporous Mater. 30 (1999) 95.

15: V.L. Zholobenko, D.B. Lukyanov, J. Dwyer, W.J. Smith, J. Phys. Chem. B 102 (1998) 2715.

16: B. Wichterlová, Z. Tvarůžková, Z. Sobalík, P. Sarv, Microporous Mesoporous Mater. 24 (1998) 223.

17: W.-Q. Xu, Y. –G. Yin, S. L. Suib, J. C. Edwards, C.-L. O'Young, J. Catal., 163 (1996) 232.

18: B. Wichterlová, N. Žilkova, E. Uvarova, J. Čejka, P. Sarv, C. Paganini, J.A. Lercher, Appl. Catal. A 182 (1999) 297.

19: G. Onyestyák, Microporous Mesoporous Mater. 104 (2007) 192.

20: K. Frolich, R. Bulánek, P. Nachtigall, Proceedings of the 40th Symposium on Catalysis, Prague, 2008, p. 40.

21: A.B. Pinar, C. Márquez-Álvarez, M. Grande-Casas, J. Pérez-Pariente, manuscript submitted to J. Catal.

22: A.B. Pinar, J. Pérez-Pariente, L. Gómez-Hortigüela, world patent WO 2008/116958.

23: L. Schereyeck, P. Caullet, J. C. Mougenel, J. L. Guth, B. Marler, Microporous Mater. 6 (1996) 259.

24: A. Burton, R. J. Accardi, R. F. Lobo, M. Falcioni, M.W. Deem, Chem. Mater. 12 (2000) 2936.

25: R. Millini, L. C. Carluccio, A. Carati, G. Bellussi, C. Perego, G. Cruciani, S. Zanardi, Microporous Mesoporous Mater. 74 (2004) 59.

26: L.M. Knight, M.A. Miller, S.C. Koster, M.G. Gatter, A.I. Benin, R.R. Willis, G.J. Lewis, R.W. Broach, Stud. Surf. Sci. Catal. 170 (A) (2007) 338.

27: R. García, L. Gómez-Hortigüela, I. Díaz, E. Sastre, J. Pérez-Pariente, Chem. Mater. 20 (2008) 1099.

28: R.Garcia, A.B. Pinar, C. Márquez-Álvarez, E.Sastre, J.Pérez-Pariente, Collect. Czech. Chem. Commun. 73 (2008) 1089.

29: C.J. Plank, E.J. Rosinski, M.K. Rubin, US Patent 4 016 245 (1977).

30: A.B. Pinar, L. Gómez-Hortigüela, J. Pérez-Pariente, Chem. Mater. 19 (2007) 5617.

31: E.P. Parry, J. Catal. 2 (1963) 371.

32: T.R. Hughes, H.M. White, J. Phys. Chem. 71 (1967) 2192.

33: Y.S. Jin, A. Auroux, J.C. Vedrine, Appl. Catal. 37 (1988) 1

34: M. Trombetta, G. Busca, S. Rossini, V. Piccoli, U. Cornaro, A. Guercio, R. Catani, R.J. Willey, J. Catal. 179 (1998) 581.

35: V.L. Zholobenko, E.R. House, Catal. Lett. 89 (2003) 35.

36: L. Domokos, L. Lefferts, K. Seshan, J.A. Lercher, J. Mol. Catal. A 162 (2000) 147.

37: M.A. Asensi, A. Martínez, Appl. Catal. A 183 (1999) 155.

38: M. A. Asensi, A. Corma, A. Martínez, J. Catal. 158 (1996) 561.

39: L. A. Villaescusa, M. A. Camblor, Recent Res. Dev. Chem., 1 (2003) 93.

FIGURE CAPTIONS

Figure 1. XRD patterns of selected (1) as-prepared and (2) calcined samples: a) FER-bmp-quin-10d, b) FER-bmp-TEA-11d, c) FER-bmp-quin-30d, d) FER-bmprol-TMA-20d, e) FER-pyrr-10d.

Figure 2. Thermogravimetric analysis of as-synthesised samples a) FER-bmp-quin-10d, b) FER-bmprol-TMA-20d, c) FER-pyrr-10d.

Figure 3. FTIR spectra in the ν_{OH} region (left) and difference spectra in the pyridine ring vibrations region (right) of calcined samples FER-bmp-TMA-20d (a), FER-bmprol-TMA-20d (b), FER-bmp-TEA-11d (c), FER-bmp-quin-10d (d) and FER-bmp-quin-30d (e). The spectra of the samples outgassed at 400ºC are shown in full thick line. Spectra recorded after pyridine adsorption at 150ºC for increasing periods of time are shown in dotted line (5 and 30 min) and full thin line (90 min).

Figure 4. Conversion (a), selectivity to isobutene (b), isobutene yield (c) and selectivity to isobutene as a function of the conversion (d) for the low-defect samples.

Figure 5. Conversion (a), selectivity to isobutene (b), isobutene yield (c) and selectivity to isobutene as a function of the conversion (d) for the high-defect samples. The low-defect sample FER-bmprol-TMA sample is included for comparison purposes.

FIGURES

Figure 1.

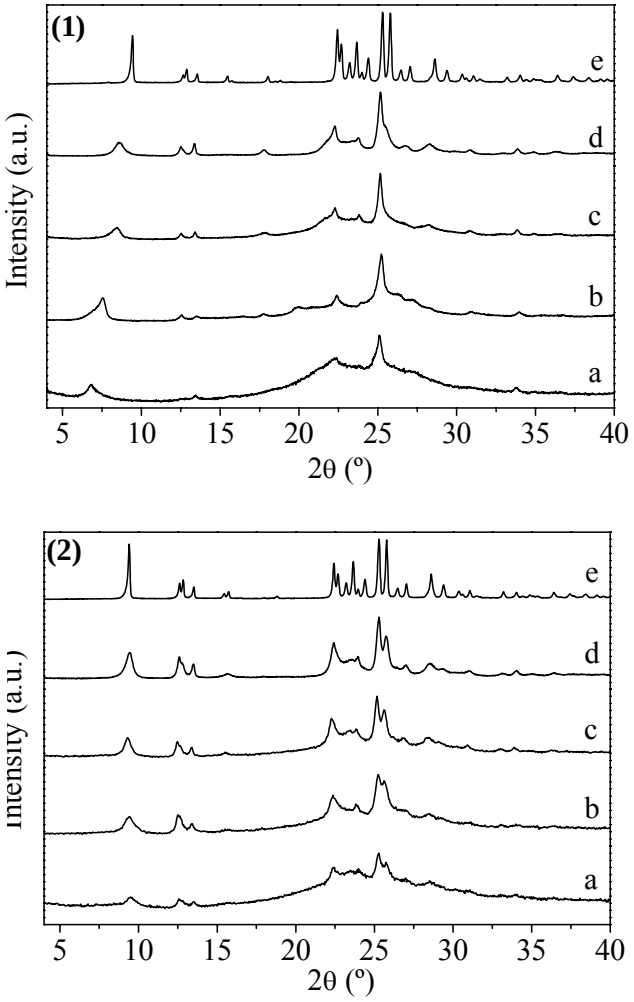

Figure 2.

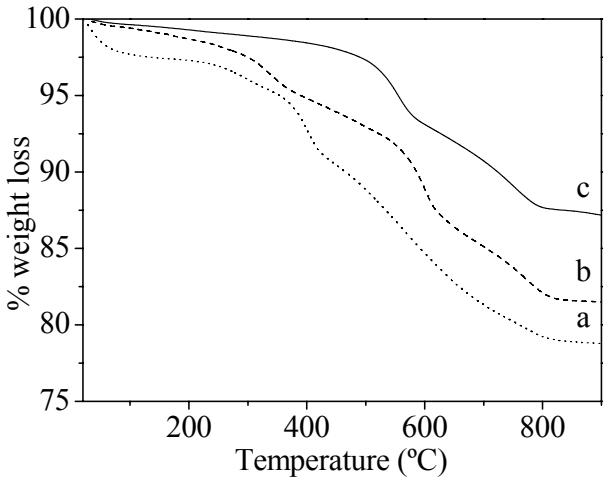
100
95
90
85
80
75
% weight loss
200
400
600
800
Temperature (ºC)
c
b
a

Figure 3.

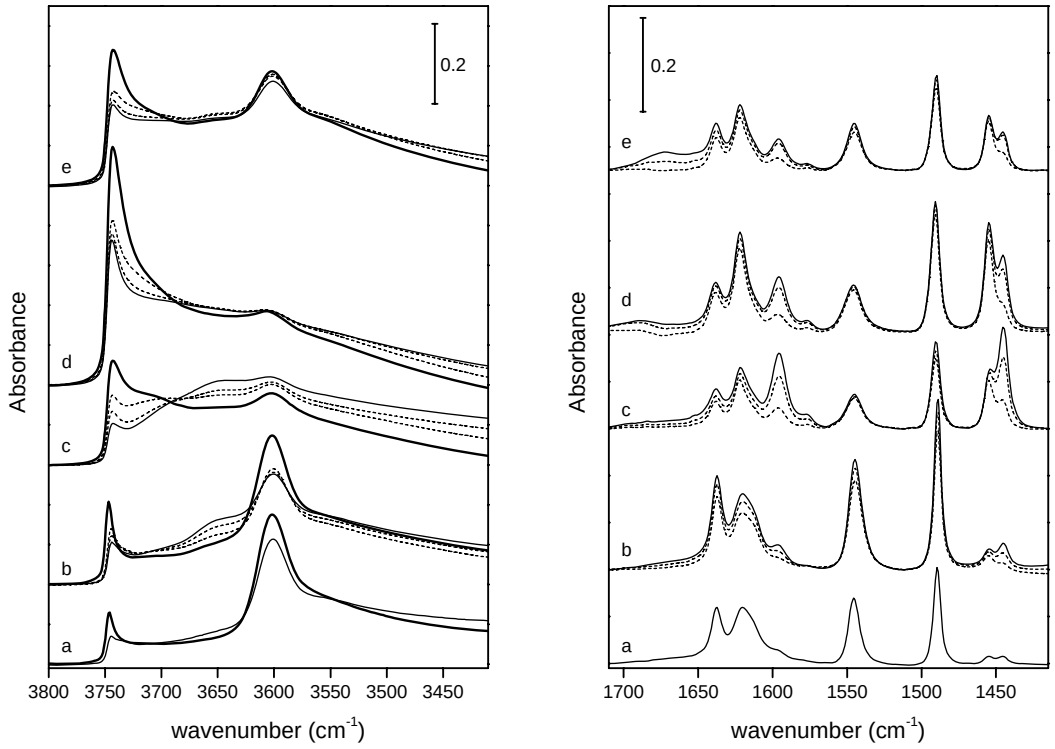
0.2
e
d
c
b
a
Absorbance
3800 3750 3700 3650 3600 3550 3500 3450
wavenumber (cm-1)
0.2
e
d
c
b
a
Absorbance
1700 1650 1600 1550 1500 1450
wavenumber (cm-1)

Figure 4.

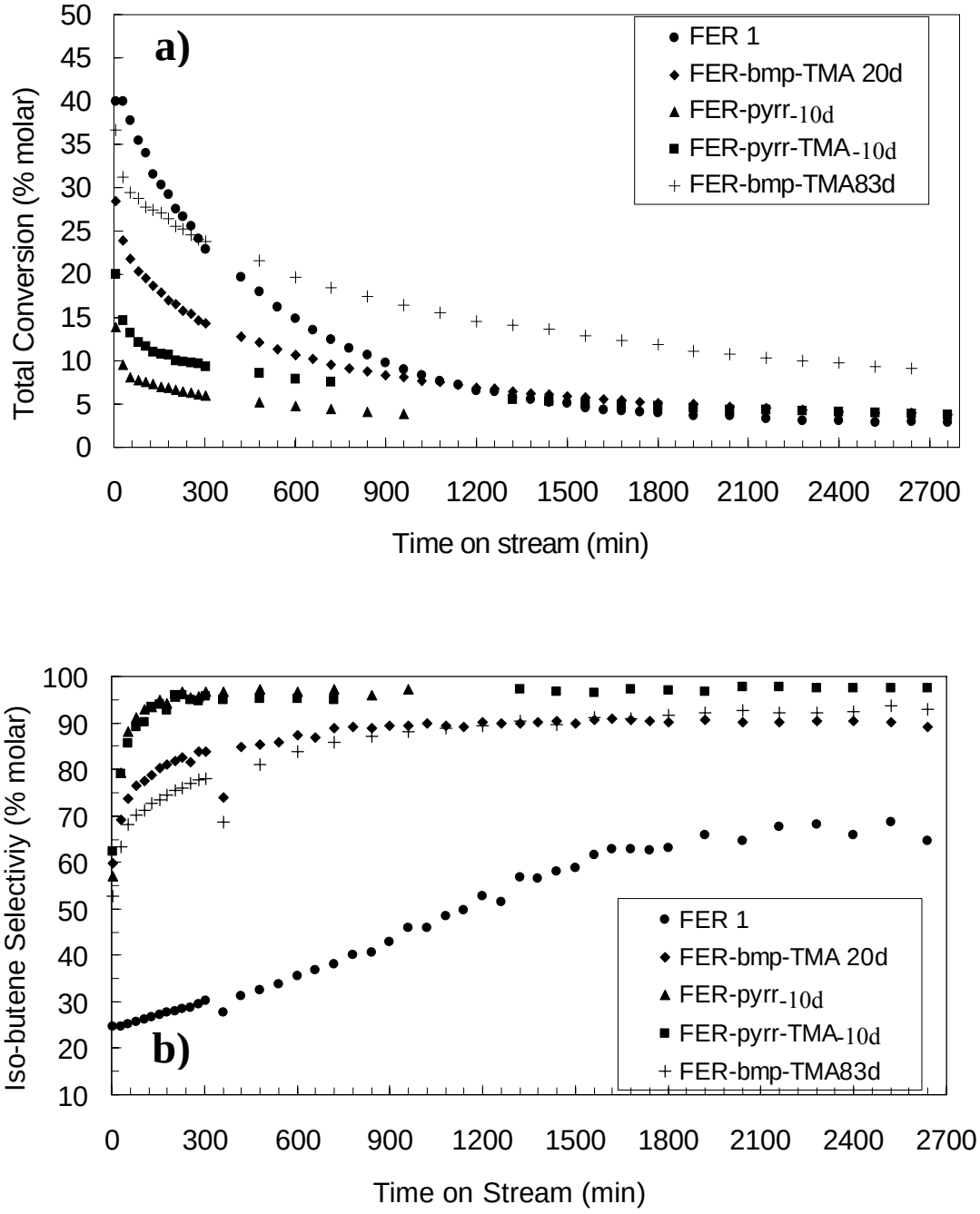
a)
Total Conversion (% molar)
Time on stream (min)
FER 1
FER-bmp-TMA 20d
FER-pyrr-10d
FER-pyrr-TMA-10d
FER-bmp-TMA83d
b)
Iso-butene Selectiviy (% molar)
Time on Stream (min)

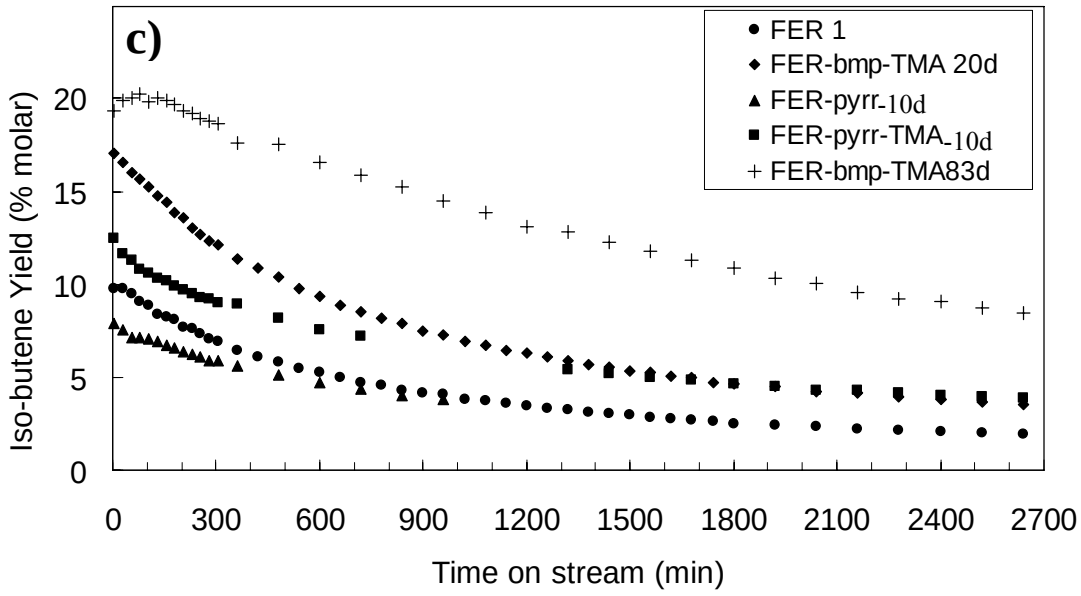
c)
FER 1
FER-bmp-TMA 20d
FER-pyrr-10d
FER-pyrr-TMA-10d
FER-bmp-TMA83d
Iso-butene Yield (% molar)
0
5
10
15
20
0
300
600
900
1200
1500
1800
2100
2400
2700
Time on stream (min)

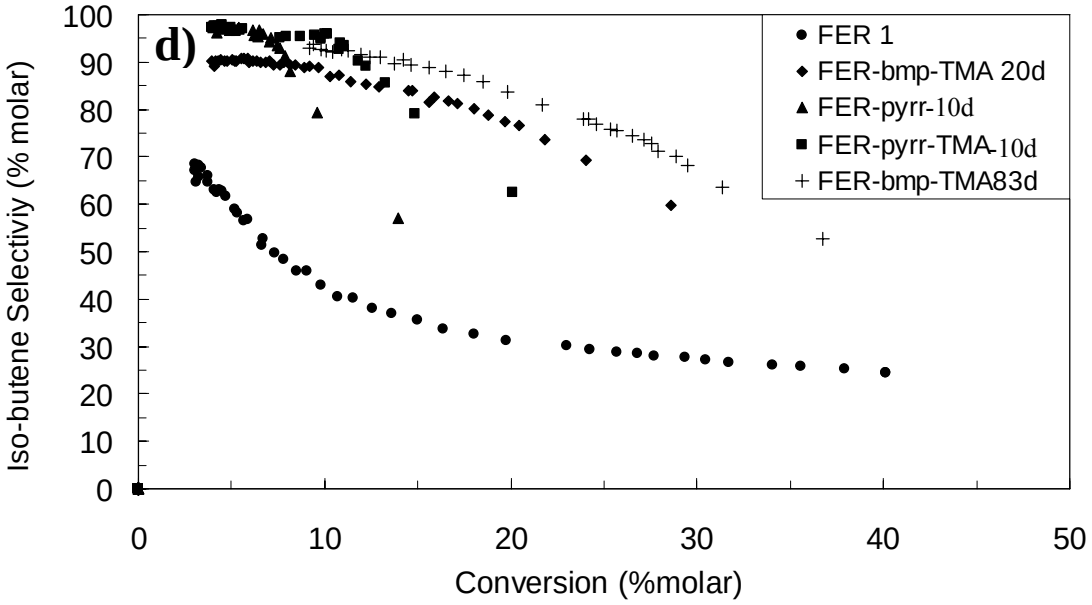
d)
FER 1
FER-bmp-TMA 20d
FER-pyrr-10d
FER-pyrr-TMA-10d
FER-bmp-TMA83d
Iso-butene Selectiviy (% molar)
0
10
20
30
40
50
60
70
80
90
100
0
10
20
30
40
50
Conversion (%molar)

Figure 5.

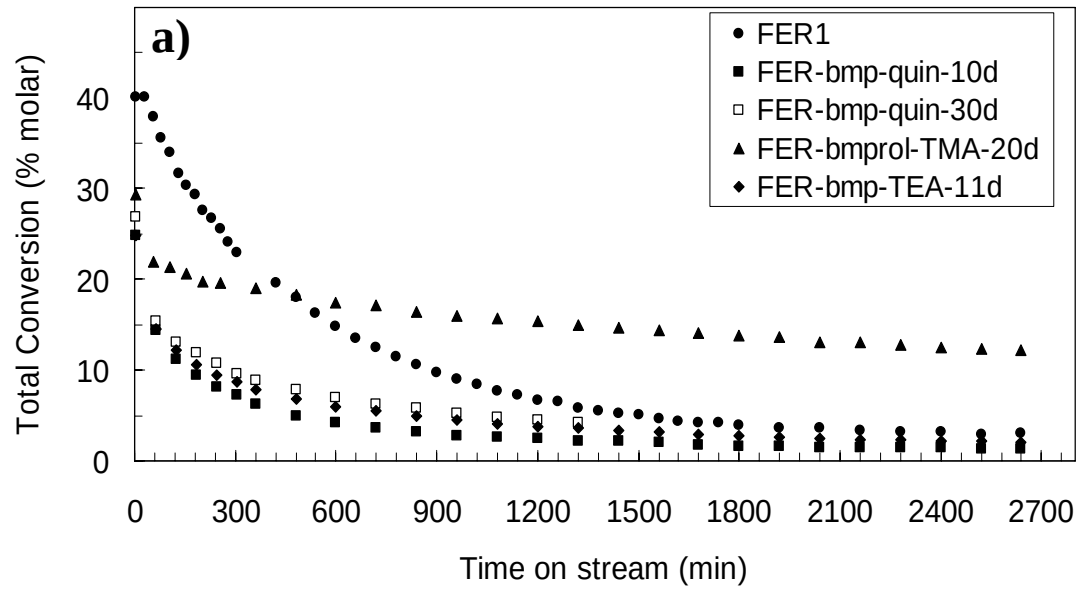
a)
Total Conversion (% molar)
0
10
20
30
40
0
300
600
900
1200
1500
1800
2100
2400
2700
Time on stream (min)
FER1
FER-bmp-quin-10d
FER-bmp-quin-30d
FER-bmprol-TMA-20d
FER-bmp-TEA-11d

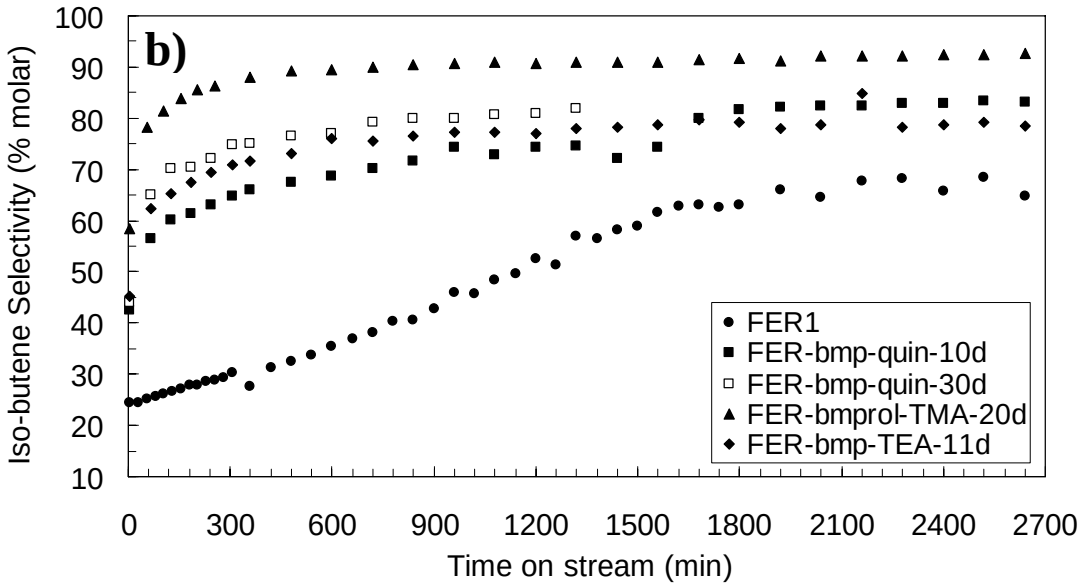
b)
Iso-butene Selectivity (% molar)
10
20
30
40
50
60
70
80
90
100
0
300
600
900
1200
1500
1800
2100
2400
2700
Time on stream (min)
FER1
FER-bmp-quin-10d
FER-bmp-quin-30d
FER-bmprol-TMA-20d
FER-bmp-TEA-11d

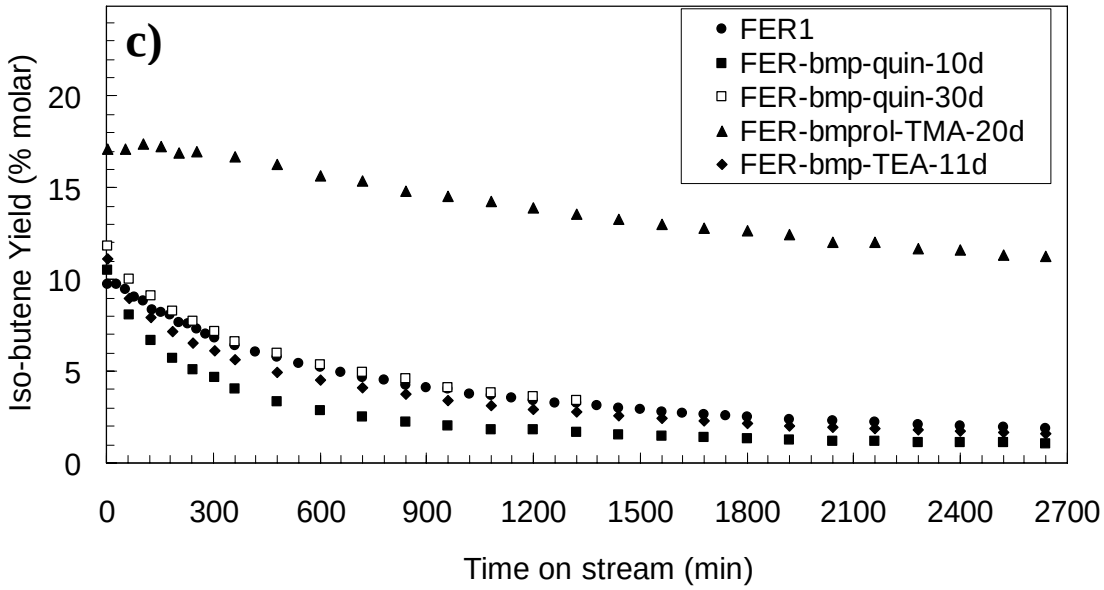
c)
FER1
FER-bmp-quin-10d
FER-bmp-quin-30d
FER-bmprol-TMA-20d
FER-bmp-TEA-11d
Iso-butene Yield (% molar)
0
5
10
15
20
0
300
600
900
1200
1500
1800
2100
2400
2700
Time on stream (min)

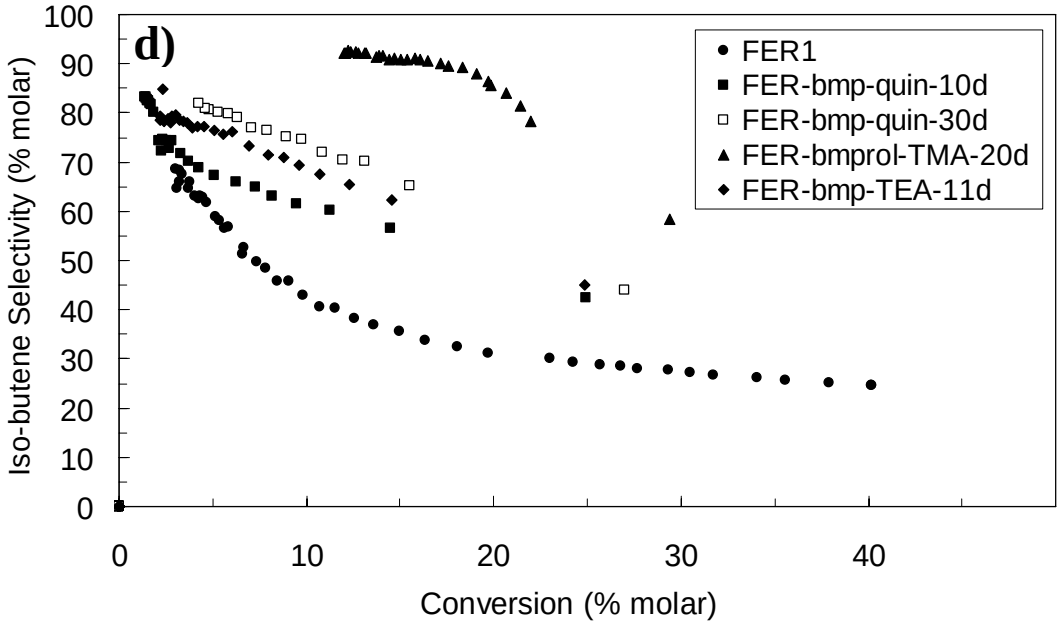
d)
FER1
FER-bmp-quin-10d
FER-bmp-quin-30d
FER-bmprol-TMA-20d
FER-bmp-TEA-11d
Iso-butene Selectivity (% molar)
0
10
20
30
40
50
60
70
80
90
100
0
10
20
30
40
Conversion (% molar)

TABLES

Table 1. Summary of the syntheses carried out with the different combinations of SDAs and Si/Al ratio of the solid products obtained. The gels compositions were: 0.06 co-SDA: 0.48 ROH: 0.48 HF : 0.03 Al_2O_3 : 0.94 SiO_2 : 4.3-4.7 H_2O, heated at 135ºC. The ferrierite-type samples were heated at 150 ºC (except FER1 sample, heated at 175 ºC) and the fully-condensed samples were heated at 135 ºC.

Sample	ROH	co-SDA	t (days)	Si/Al(EDX)	Product
Ferrierite-type materials					
FER-bmp-quin-10d	bmp	quin	10	14.6[a]	FER-related
FER-bmp-quin-30d	bmp	quin	30	15.5[a]	FER-related
FER-bmp-TEA-11d	bmp	TEA	11	18.6	FER-related
FER-bmprol-TMA-20d	bmprol	TMA	20	15.8	FER-related
Fully-condensed ferrierite					
FER-bmp-TMA-20d	bmp	TMA	20	15.5	Ferrierite
FER-bmp-TMA-83d	bmp	TMA	83	15.6	Ferrierite
FER-pyrr-TMA-10d	pyrr	TMA	10	15.9	Ferrierite
FER-pyrr-10d	pyrr	-	10	15.0	Ferrierite
FER1	pyrr	-	14	15.8	Ferrierite

a: ICP analysis

Table 2. Organic content and thermogravimetric analysis data of as-synthesised samples, and BET surface area of calcined materials.

Sample	Chemical analysis (wt.%)			TGA[a]	
	C	H	N	wt.%	S_{BET} (m^2/g)
Ferrierite-type materials					
FER-bmprol-TMA-20d	9.38	2.05	1.73	17.1	261
FER-bmp-TEA-11d	13.87	2.68	1.75	20.9	285
FER-bmp-quin-10d	12.51	2.32	1.55	18.5	446
FER-bmp-quin-30d	11.75	2.20	1.75	17.9	374
Fully-condensed ferrierite					
FER-bmp-TMA-20d	9.30	1.83	1.73	13.7	305
FER-bmp-TMA-83d	8.40	1.66	1.62	11.7	-
FER-pyrr-TMA-10d	7.58	1.86	1.97	11.6	341
FER-pyrr-10d	7.35	1.74	2.00	11.2	350
FER1	5.48	1.38	1.61	9.6	244

[a] Weight loss in the range 200-900 ºC as measured by thermogravimetric analysis, associated to the decomposition/combustion of organic material and removal of silanol groups as water.

Table 3. FTIR characterisation of acid sites [a]

Sample	Brönsted sites accessibility [b] (%)	Py-B band area [c] (cm^{-1})	Py-L band area [d] (cm-1)
FER1	52	1.74	0.12
FER-pyrr-10d	10	0.95	0.05
FER-pyrr-TMA-10d	18	1.59	0.05
FER-bmp-TMA-20d	36	1.31	0.12
FER-bmprol-TMA-20d		2.48	0.48
FER-bmp-TEA-11d		1.13	1.86
FER-bmp-quin-10d		1.50	1.57
FER-bmp-quin-30d		1.31	0.80

[a] Data obtained by adsorption of pyridine at 150ºC for 90 min

[b] Decrease of intensity of the bridging hydroxyl band at 3601 cm^{-1}

[c] Area of the pyridinium band (1545 cm^{-1})

[d] Area of the pyridine coordinated to Lewis sites (1455 cm^{-1})

Table 4. Catalytic activity in the n-butene isomerisation for the low-defect samples.

Samples	FER1		FER-bmp-TMA-20d		FER-bmp-TMA-83d		FER-bmprol-TMA-20d		FER-pyrr-10d		FER-pyrr-TMA-10d	
Time (min.)	5	720	5	720	5	720	5	720	5	720	5	720
Conversion (% molar)	40.15	12.54	28.58	9.66	36.67	18.52	29.42	17.16	13.95	4.52	20.07	7.61
						Selectivity (% molar)						
C1	0.00	0.00	0.00	0.00	0.00	0.00	0.00	0.00	0.13	0.00	0.10	0.00
C2	0.00	0.00	0.00	0.00	0.00	0.00	0.00	0.00	0.13	0.00	0.00	0.00
$C2^{=}$	0.83	0.18	1.09	0.00	1.16	0.00	1.13	0.00	2.83	0.00	2.11	0.00
C3	0.86	0.15	0.81	0.00	1.10	0.00	0.80	0.00	1.51	0.00	1.07	0.00
$C3^{=}$	27.45	21.16	16.61	1.56	17.28	2.02	14.71	1.79	22.97	0.62	19.36	0.61
I-C4	1.10	0.73	0.73	0.37	2.09	0.30	1.02	0.28	0.35	0.67	0.38	0.40
N-C4	1.67	1.26	4.27	0.78	3.94	0.68	3.58	0.70	4.21	0.79	3.69	0.59
$I\text{-}C4^{=}$	24.55	38.16	59.88	88.88	52.77	85.92	58.46	89.99	57.05	97.28	62.43	95.00
C5	1.58	0.31	0.18	0.00	0.55	0.00	0.17	0.00	0.24	0.00	0.19	0.00
$C5^{=}$	26.07	23.37	12.94	2.00	16.04	2.79	10.77	2.07	9.06	0.64	9.02	0.63
C6	13.08	6.86	2.49	0.00	3.65	0.00	2.25	0.00	1.40	0.00	1.34	2.77
C7	2.82	2.77	1.00	0.00	1.44	0.17	7.12	5.16	0.15	0.00	0.32	0.00
>C7	0.00	5.05	0.00	6.40	0.00	8.12	0.00	0.00	0.00	0.00	0.00	0.00

Table 5. Catalytic activity in the n-butene isomerisation for the high defect samples.

Samples	FER-bmp-quin-10d		FER-bmp-quin-30d		FER-bmp-TEA-11d	
Time (min.)	5	720	5	720	5	720
Conversion (% molar)	24.92	3.71	26.99	6.33	24.88	5.56
	Selectivity (% molar)					
C1	0.00	0.00	0.00	0.00	0.00	0.00
C2	0.00	0.00	0.00	0.00	0.00	0.00
C2=	0.74	0.00	1.36	0.00	0.86	0.00
C3	0.81	0.00	1.24	0.00	0.63	0.00
C3=	16.80	7.86	18.06	4.40	16.19	4.73
I-C4	5.15	1.34	3.72	0.00	2.78	0.00
N-C4	2.31	1.29	3.73	2.33	2.79	2.62
I-C4=	42.45	70.23	44.11	79.18	45.13	75.58
C5	1.28	0.00	0.77	0.00	0.66	0.00
C5=	18.40	10.51	15.81	6.25	17.21	6.57
C6	3.44	0.00	3.04	0.00	2.98	0.00
C7	8.63	8.78	8.16	7.84	10.77	10.50
>C7	0.00	0.00	0.00	0.00	0.00	0.00